Modeling the Electromagnetic Fields of 25 kV Traction Networks Under Emergency Conditions

Konstantin Suslov *, Andrey Kryukov, Ekaterina Voronina, Azat Akhmetshin

Posted Date: 6 June 2023

doi: 10.20944/preprints202306.0400.v1

Keywords: power supply systems for AC railways; emergency conditions; electromagnetic fields near supports; modeling; electromagnetic safety

Article

Modeling the electromagnetic fields of 25 kV traction networks under emergency conditions

K. V. Suslov [1,2,*], A. V. Kryukov [2,3], E. V. Voronina [3] and Azat Akhmetshin [4]

[1] Department of Hydropower and Renewable Energy, National Research University "Moscow Power Engineering Institute", Moscow, Russia
[2] Department of Power Supply and Electrical Engineering, Irkutsk National Research Technical University, Irkutsk, Russia; and_kryukov@mail.ru
[3] Department of Transport Electric Power, Irkutsk State Transport University, Irkutsk, Russia
[4] Department of Power Engineering, Kazan State Power Engineering University, 420066, Kazan, Russia; dr.akhmetshin@ieee.org
* Correspondence: dr.souslov@yandex.ru; Tel.: +7-914-8704673

Abstract: When in operation, the 25 kV traction networks may encounter the contact wire short circuits to rails or ground. The short-circuit conditions cause high-intensity magnetic fields (EMFs), which, despite the short duration of exposure, can negatively affect electronic devices and lead to significant induced voltage on adjacent power lines. There can be two main types of emergency conditions in 25 kV traction networks: the contact wire short circuit to the rail, when the supports are grounded to the rail track; and the contact wire short circuit to the ground in sections with supports disconnected from the rails. A three-dimensional electromagnetic field near a metal support when a short-circuit current flows through it is characterized by a complex spatial structure, which significantly complicates the calculations of intensities. The paper discusses the results of computer modeling aimed at determining the EMF intensity in the described emergencies. The objects involved in modeling were represented by segments of thin wires to calculate the electric charge distribution and find out the EMF intensity. This approach is implemented in the Fazonord software. The modeling results have shown that EMF intensities near the support grow significantly; their levels decrease noticeably as one moves away from the support; and that the three-dimensional electromagnetic field under the considered emergency conditions has a complex spatial structure.

Keywords: power supply systems for AC railways; emergency conditions; electromagnetic fields near supports; modeling; electromagnetic safety

1. Introduction

Electromagnetic fields are among the main factors that determine the conditions of electromagnetic safety at electric power facilities, including transport [1,2]. They can generate interference that disrupts the normal functioning of electrical and electronic devices [2], cause ignition of flammable substances, and lead to serious accidents at work of personnel on disconnected power and communications lines due to effect of induced voltages.

There is also a direct negative effect of EMF on humans [1], which inhibits processes in the central nervous system and causes headache, lethargy, and fatigue. There are also changes in blood composition and pressure, and an increase in heart rate. Capacitance currents at high EMF intensity can change the metabolic process. Industrial frequency fields have a particularly great influence on people, since with an increase in frequency, there is an effect of inertia of the opening of cell membranes, and with its decrease, induced and capacitance currents go down.

Traction networks (TN) of electrified AC railways are among the serious EMF sources due to electromagnetic imbalance. The electromagnetic interference of the traction network causes large voltage in adjacent devices. This voltage can cause severe equipment damage and electrical injury.

 doi:10.20944/preprints202306.0400.v1

A large number of studies are concerned with the modeling of electromagnetic fields of power transmission lines and traction networks. The article [3] considers the f use of the Comsol Multiphysics software modules in calculating electromagnetic fields generated near high-voltage power lines. The work [4] analyzes the electromagnetic fields along the route of a high-voltage transmission line, and presents the results of the analysis of the influence of key variables on the EMF intensity. The findings of the study on the electromagnetic field between the power line and the railway are presented in [5]. In [6], the authors focus on the electromagnetic fields of 132 kV transmission lines, which were calculated using the Biot-Savart law and Maxwell's equations. To simplify the calculation of the magnetic field, the superposition method was applied. In [7], the magnitude of the EMF intensity is shown to depend on the distance between the supports. In addition, it presents the results of theoretical studies related to the absorption of electromagnetic energy and the evaluation of the effectiveness of measures to protect personnel from the EMF effects. The article [8] presents data characterizing the EMF levels under the 500 kV lines. The simulation was performed for horizontal and vertical conductor arrangement under balanced and unbalanced conditions. The results of the analysis of the EMF distribution at high-voltage substations are given in [9]. The authors of [10] present a model for examining the industrial frequency electromagnetic field created by a high-voltage transmission line. The distribution of the electric field along the route of a 400 kV power transmission line is analyzed in [11]. The levels of influence of an electric field caused by high-voltage power lines on a human are assessed in [12]. The results of modeling the electric field of 330 kV power transmission lines located near buildings are presented in [13]. The study [14] developed a technique for modeling the electromagnetic field of a traction network near contact networks and rails. The method for calculating the low-frequency electromagnetic field around 15 kV power lines is proposed in [15]. The calculation results for electromagnetic fields of overhead transmission lines are given in [16]. Electromagnetic fields around power lines of various designs are compared in [17]. The findings of the research into EMF at the Xijiang traction substation are given in [18]. The influences of the electromagnetic field produced by an electrified railway section are analyzed in [19]. Methods for predicting electromagnetic fields in the territories of high-voltage substations based on fuzzy models are described in [20]. The electromagnetic fields of substations are analyzed in [21,22]. The issues of electromagnetic compatibility and safety on the routes of electrified railways are considered in the monograph [23] and article [24]. Electromagnetic fields produced by high-speed transport systems are analyzed in [25]. The aspects of modeling and measuring parameters that determine the conditions for electromagnetic compatibility and safety at railway electrical substations are examined in [26]. The results of simulation and analysis of the electromagnetic environment of traction networks are presented in [27].

An analysis of the described publications suggests that they address very important aspects of determining EMF produced by power lines and traction networks and analyze electromagnetic safety conditions. However, the publications discussed do not provide a method for modeling EMF near the metal supports of the catenary system under emergency conditions. Such a method can be implemented based on the algorithms given in [28] and implemented in the Fazonord software [29].

2. Problem Statement

There can be two main types of emergency conditions in 25 kV traction networks: contact suspension short circuit to the rail, when the supports are grounded to the rail track; and contact suspension short circuit to the ground in sections with supports disconnected from the rails. Grounding the supports of the contact network on the rail track reduces the reliability of the track circuits and complicates the track work without removing the voltage due to the need to disconnect the grounding leads from the rails [30]. If the spreading resistance of the support foundation is less than 100 Ohm, it is required to connect it to the rail through an earth arrester, which requires a large amount of work to check and replace faulty arresters. The study [30] shows that for the majority of practically significant conditions, the probability of hazardous situations in sections with supports disconnected from the rails is considerably lower than the same indicator for sections with supports connected to them.

 doi:10.20944/preprints202306.0400.v1

A three-dimensional electromagnetic field near a metal support with a short-circuit current flowing through it is characterized by a complex spatial structure, which significantly complicates the calculations of intensity. The EMF near supports under emergency conditions can be determined using the approach proposed in [28] and implemented in the Fazonord software [29]. In this case, the current-carrying parts were represented by segments of thin wires to calculate the distribution of electric charge and further calculate the intensities of the electric and magnetic fields.

The proposed approach has the following features that significantly distinguish it from the above-described methods designed to determine the electromagnetic fields of power transmission lines and traction networks:

- electromagnetic fields can be calculated for traction networks of various designs, for example, 25, 2x25 kV, traction networks equipped with shielding wires, line feeders, suction transformers, etc.;
- a systems approach to EMF modeling is implemented because EMF determination involves the power flow calculation for a complex electric power system or a traction power supply system;
- the method allows determining the technical efficiency of devices used to reduce EMF intensities, for example, shielding wires.
- Below is a brief description of the algorithms used in the modeling.

3. Modeling Method

The EMF of short wires can be modeled by representing such objects as a series of parts connected successively to calculate the electric charge distribution and further determine the intensities of the electric and magnetic fields [28]. It is necessary to calculate power flow of the electrical system first, as it determines the current and voltage of the wires.

Modeling is based on the following main propositions:

- the objects under consideration are segments of thin straight wires arbitrarily located in space;
- some current-carrying parts (e.g., cables) can be buried;
- the size of the set of objects must be limited to operate with the concepts of electrical circuits and the equations of the quasi-stationary zone; for a frequency of 50 Hz and significant harmonics, these dimensions should not exceed the first hundreds of meters.

A careful analysis of the problem at issue raises a difficult question whether it is possible to use the concepts of self-inductance and mutual inductance of short wire segments. These concepts imply the presence of corresponding loops with magnetic fluxes. The problem of determining such loops for short segments is not trivial, since the magnetic field in this situation ceases to be plane-parallel. However, mutual inductive influences can be excluded from consideration for the current-carrying parts with a length of the order of several tens of meters.

This approach can be justified by the following. The induced voltage due to mutually inductive couplings can be estimated using the formulas [31,32] for long and parallel wires. If we consider extreme cases with single-phase short-circuit currents reaching 50 kA, with distances between the wires of 20 m and a length of the affected wire of 50 m, then the induced electromotive force of magnetic influence will be 610 V. This value conservatively places upper limits on the possible induced voltage of magnetic influence; a decrease in the influencing current and the length of the affected wire reduces the induced electromotive force proportionally. The induced voltage at operating currents of the order of 1 kA is limited from above by a value of about 12 V, which makes it possible not to factor in mutually inductive couplings between individual short wires. Symmetrical short circuits, as well as edge effects of short current-carrying parts, will lead to much lower values of induced voltage. Under normal load conditions, the effects of mutually inductive couplings can be neglected. There will also be no induced voltage in the case of a mutually perpendicular arrangement of wires. This in particular means that the potentials of grounded objects in the absence of working or emergency currents in them can be taken as zero; these objects nevertheless will determine the structure of the electric field.

Following the logic of the Fazonord software [29], the EMF calculation for short wires assumes that the result of power flow calculation for the system, which they belong to, is known. Due to the

Preprints (www.preprints.org) | NOT PEER-REVIEWED | Posted: 6 June 2023 doi:10.20944/preprints202306.0400.v1

small influence of short wires on the power flow, calculation of the latter involves their modeling similarly to long current-carrying parts. By calculating the power flow, we determine the voltage and current of short wires, which are necessary to find out the intensities of the electric and magnetic fields. The calculation formulas applied further and the algorithm for determining the EMF intensities are presented below.

Figure 1 shows the coordinate system and a single short wire. The location of the X0Z plane is chosen so that it coincides with the plane of the earth's surface. The current system assumes N_w short wires, in each of which operating or emergency currents flow. In addition, earthed conductive objects without current are taken into account. Each short wire i has length L and is divided into a number n_i of line elements, each of which has length $\Delta l_i = L_i / n_i$. In some cases, below, the length of a line element is denoted by Δl_{ij} to indicate with index j the location of the element on wire i; the numbering of the line elements starts with unity from the beginning of wire 1 according to Figure 1. Magnitude Δl_{ij} does not depend on j.

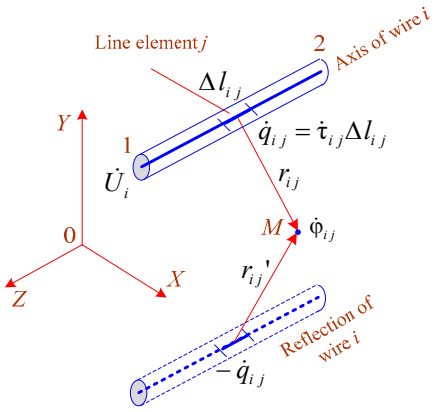

Figure 1. To the calculation of the electric field of a line element of the wire.

Wire i creates at the observation point M, having coordinates (x, y, z), potential determined by the formula:

$$\dot{\varphi}_i = \frac{1}{4\pi\varepsilon_0}\int_0^{L_i}\left[\left(\frac{1}{r}-\frac{1}{r'}\right)\dot{\tau}_i\, dl_{ij}\right] \approx \frac{1}{4\pi\varepsilon_0}\sum_{j=1}^{n_i}\left(\frac{1}{r_{ij}}-\frac{1}{r_{ij}'}\right)\dot{q}_{ij} \qquad (1)$$

where r_{ij} – a distance from the middle of segment Δl_{ij} to the observation point, $r_{ij'}$ – a distance from the middle of the mirror image of line element Δl_{ij} to the observation point, $\dot{q}_{ij} = \dot{\tau}_{ij}\Delta l_{ij}$ – charge complex of line element j of wire i; n_i – the number of line elements of the wire. When choosing equivalent charges in the form of point charges, the values r_{ij} and r_{ij}' are determined through the given coordinates of the beginning x_{i1}, y_{i1}, z_{i1} and end x_{i2}, y_{i2}, z_{i2} of the short wire:

$$r_{ij} = \sqrt{[x - x_{i1} - (j-0{,}5)\Delta x_i]^2 + [y - y_{i1} - (j-0{,}5)\Delta y_i]^2 + [z - z_{i1} - (j-0{,}5)\Delta z_i]^2};$$

$$r_{ij}' = \sqrt{[x - x_{i1} - (j-0{,}5)\Delta x_i]^2 + [y + y_{i1}' + (j-0{,}5)\Delta y_i]^2 + [z - z_{i1} - (j-0{,}5)\Delta z_i]^2};$$

where $\Delta x_i = (x_{i2} - x_{i1})/n_i$; $\Delta y_i = (y_{i2} - y_{i1})/n_i$; $\Delta z_i = (z_{i2} - z_{i1})/n_i$.

The choice of an equivalent charge located on the wire axis is more efficient than representation by point charges. Potential created at the observation point by the axis of the line element j with length Δl_i of wire i with charge density $\dot{\tau}_{ij}$ and the reflection of the line element in the ground (Figure 2) is equal to

Preprints (www.preprints.org) | NOT PEER-REVIEWED | Posted: 6 June 2023 doi:10.20944/preprints202306.0400.v1

$$\dot{\varphi}_{ij} = \frac{\dot{\tau}_{ij}}{4\pi\varepsilon_0} \ln \frac{(r_{ij1} + r_{ij2} + \Delta l_i)\,(r_{ij1}' + r_{ij2}' - \Delta l_i)}{(r_{ij1} + r_{ij2} - \Delta l_i)\,(r_{ij1}' + r_{ij2}' + \Delta l_i)} \tag{2}$$

where r_{ij1}, r_{ij2}, r_{ij1}', r_{ij2}' – distance from the beginning and end of the line element j and from the beginning and end of its reflection to the observation point M, defined as follows:

$$r_{ij1} = \sqrt{[x - x_{i1} - (j-1)\Delta x_i]^2 + [y - y_{i1} - (j-1)\Delta y_i]^2 + [z - z_{i1} - (j-1)\Delta z_i]^2}\ ;$$

$$r_{ij2} = \sqrt{[x - x_{i1} - j\,\Delta x_i]^2 + [y - y_{i1} - j\,\Delta y_i]^2 + [z - z_{i1} - j\,\Delta z_i]^2}\ ;$$

$$r_{ij1}' = \sqrt{[x - x_{i1} - (j-1)\Delta x_i]^2 + [y + y_{i1} + (j-1)\Delta y_i]^2 + [z - z_{i1} - (j-1)\Delta z_i]^2}\ ;$$

$$r_{ij2}' = \sqrt{[x - x_{i1} - j\,\Delta x_i]^2 + [y + y_{i1} + j\,\Delta y_i]^2 + [z - z_{i1} - j\,\Delta z_i]^2}\ .$$

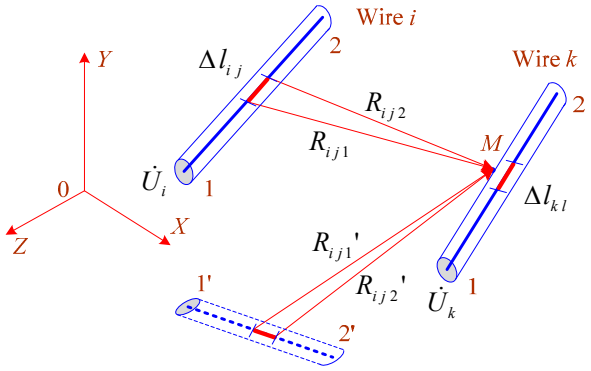

Figure 2. Scheme of the contribution of the line element Δl_{ij} to the potential of segment Δl_{kl}.

It is possible to build a system of equations using the method of equivalent charges to calculate the complex value $\dot{\tau}_{ij}$ of wire i of line element j:

$$\begin{cases} \alpha_{11}\dot{\tau}_1 + \ldots + \alpha_{1,n1}\dot{\tau}_{n1} + \alpha_{1,n1+1}\dot{\tau}_{n1+1} + \ldots + \alpha_{1,Ns}\dot{\tau}_{Ns} = 4\pi\varepsilon_0\dot{\varphi}_1; \\ \alpha_{21}\dot{\tau}_1 + \ldots + \alpha_{2,n1}\dot{\tau}_{n1} + \alpha_{2,n1+1}\dot{\tau}_{n1+1} + \ldots + \alpha_{2,Ns}\dot{\tau}_{Ns} = 4\pi\varepsilon_0\dot{\varphi}_1; \\ \ldots\ldots\ldots\ldots\ldots\ldots\ldots\ldots\ldots\ldots\ldots\ldots \\ \alpha_{k,1}\dot{\tau}_1 + \ldots + \alpha_{k,n1}\dot{\tau}_{n1} + \alpha_{k,n1+1}\dot{\tau}_{n1+1} + \ldots + \alpha_{k,Ns}\dot{\tau}_{Ns} = 4\pi\varepsilon_0\dot{\varphi}_k; \\ \ldots\ldots\ldots\ldots\ldots\ldots\ldots\ldots\ldots\ldots\ldots\ldots \\ \alpha_{Ns,1}\dot{\tau}_1 + \ldots + \alpha_{Ns,n1}\dot{\tau}_{n1} + \alpha_{Ns,n1+1}\dot{\tau}_{n1+1} + \ldots + \alpha_{Ns,Ns}\dot{\tau}_{Ns} = 4\pi\varepsilon_0\dot{\varphi}_{Ns}, \end{cases} \tag{3}$$

In Formulas (3), $N_S = \sum_{i=1}^{Nw} n_i$ – the sum of line elements of all short wires; we assume end-to-end indexing of values $\dot{\tau}_{ij}$: $\dot{\tau}_1$, $\dot{\tau}_2$, … $\dot{\tau}_{n1}$ are charge density for the first wire; $\dot{\tau}_{n1+1}$; $\dot{\tau}_{n1+2}$; … $\dot{\tau}_{n1+n2}$ are charge density for the second wire, etc.; the index of the last quantity and the number of equations are equal to N_S. The numbering of line elements of the wires is assumed in the same order.

Potential coefficients are calculated using the following formula:

$$\alpha_{ij} = \ln \frac{(R_{ij1} + R_{ij2} + \Delta l_i)\,(R_{ij1}' + R_{ij2}' - \Delta l_i)}{(R_{ij1} + R_{ij2} - \Delta l_i)\,(R_{ij1}' + R_{ij2}' + \Delta l_i)} \tag{4}$$

where $\alpha_{ij} \neq \alpha_{ji}$ due to possible differences in the lengths of line elements of different wires.

With line elements j and l located on different wires with numbers i and k, distances are determined by the following expressions:

Preprints (www.preprints.org) | NOT PEER-REVIEWED | Posted: 6 June 2023 doi:10.20944/preprints202306.0400.v1

$$R_{ij\,1}=\sqrt{(x_{k\,l1}-x_{ij1})^2+(y_{k\,l1}-y_{ij1})^2+(z_{k\,l1}-z_{ij1})^2}\;;$$
$$x_{k\,l1}-x_{ij1}=x_{k\,1}+(l-0{,}5)\,\Delta x_k-x_{i1}-(j-1)\,\Delta x_i\;;$$
$$y_{k\,l1}-y_{ij1}=y_{k\,1}+(l-0{,}5)\,\Delta y_k-y_{i1}-(j-1)\,\Delta y_i\;;$$
$$z_{k\,l1}-z_{ij1}=z_{k\,1}+(l-0{,}5)\,\Delta z_k-z_{i1}-(j-1)\,\Delta z_i\;;$$
$$R_{ij\,2}=\sqrt{(x_{k\,l2}-x_{ij2})^2+(y_{k\,l2}-y_{ij2})^2+(z_{k\,l2}-z_{ij2})^2}\;;$$
$$x_{k\,l2}-x_{ij2}=x_{k\,1}+(l-0{,}5)\,\Delta x_k-x_{i1}-j\,\Delta x_i\;;$$
$$y_{k\,l2}-y_{ij2}=y_{k\,1}+(l-0{,}5)\,\Delta y_k-y_{i1}-j\,\Delta y_i\;;$$
$$z_{k\,l2}-z_{ij2}=z_{k\,1}+(l-0{,}5)\,\Delta z_k-z_{i1}-j\,\Delta z_i\;;$$
$$R_{ij\,1}'\approx R_{ij\,2}'\approx\sqrt{(x_{k\,l1}-x_{ij1}')^2+(y_{k\,l1}-y_{ij1}')^2+(z_{k\,l1}-z_{ij1}')^2}\;;$$
$$x_{k\,l1}-x_{ij1}'=x_{k\,1}+(l-0{,}5)\,\Delta x_k-x_{i1}-(j-0{,}5)\,\Delta x_i\;;$$
$$y_{k\,l1}-y_{ij1}'=y_{k\,1}+(l-0{,}5)\,\Delta y_k+y_{i1}+(j-0{,}5)\,\Delta y_i\;;$$
$$z_{k\,l1}-z_{ij1}'=z_{k\,1}+(l-0{,}5)\,\Delta z_k-z_{i1}-(j-0{,}5)\,\Delta z_i\;.$$

In the event that line elements are located within the same wire, $j\neq l$, and the index of the element, near which the observation point M is located on the surface of the wire (Figure 3), is indicated by symbol l, then, assuming the proximity of the point M to the wire axis, at the line element length equal to at least several wire radii, we can write

$$R_{ij\,1}\approx\left|(l-j+0{,}5)\right|\Delta l_i\;;\quad R_{ij\,2}\approx\left|(l-j-0{,}5)\right|\Delta l_i\;. \tag{5}$$

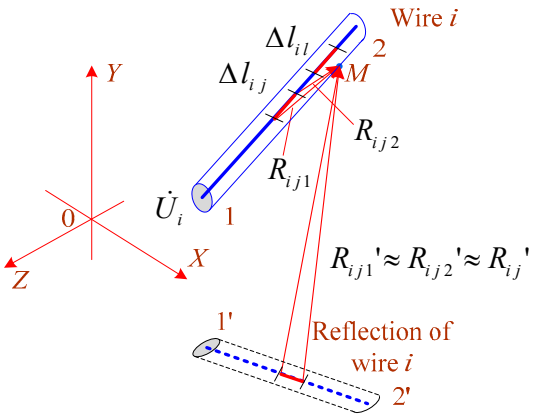

Figure 3. Line elements within one wire.

When the observation point M is located within the same wire, the contribution determined by the reflection charges can be calculated using the point charge formula

$$\alpha_{ij}=\ln\frac{R_{ij\,1}+R_{ij\,2}+\Delta l_i}{R_{ij\,1}+R_{ij\,2}-\Delta l_i}-\frac{\Delta l_i}{R_{ij}'}\;; \tag{6}$$

$$R_{ij}'\approx\sqrt{[(l-j)\Delta x_i]^2+[2y_{i1}+2(l-j)\Delta y_i]^2+[(l-j)\Delta z_i]^2}\;. \tag{7}$$

If $j=l$ (Figure 4), then Formula (6) is used and the distances within a line element are determined according to the following expression:

$$R_{ii\,1}=R_{ii\,2}=\sqrt{(0{,}5\Delta l_i)^2+R_i^{\,2}}\;, \tag{8}$$

where R_i – radius of wire i.

Preprints (www.preprints.org) | NOT PEER-REVIEWED | Posted: 6 June 2023 doi:10.20944/preprints202306.0400.v1

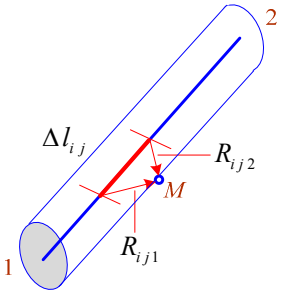

Figure 4. To determination of self-potential coefficient.

After $\dot{\tau}_{ij}$ is determined, the components of the field intensity at the observation point *M* are calculated using the formulas of point charges, $\dot{q}_{ij} = \dot{\tau}_{ij}\Delta l_i$

$$\dot{\vec{E}} = \frac{1}{4\pi\varepsilon_0}\sum_{i=1}^{Nw}\sum_{j=1}^{n_i}\dot{q}_{ij}\left(\frac{\vec{e}_r}{r_{ij}^{\,2}} - \frac{\vec{e}_r\,'}{r_{ij}'^{2}}\right), \tag{9}$$

$$r_{ij} = \sqrt{[x - x_{i1} - (j-0{,}5)\Delta x_i]^2 + [y - y_{i1} - (j-0{,}5)\Delta y_i]^2 + [z - z_{i1} - (j-0{,}5)\Delta z_i]^2};$$

$$r_{ij}' = \sqrt{[x - x_{i1} - (j-0{,}5)\Delta x_i]^2 + [y + y_{i1} + (j-0{,}5)\Delta y_i]^2 + [z - z_{i1} - (j-0{,}5)\Delta z_i]^2};$$

$$\vec{e}_r = \frac{x - x_{i1} - (j-0.5)\Delta x_i}{r_{ij}}\vec{e}_x + \frac{y - y_{i1} - (j-0.5)\Delta y_i}{r_{ij}}\vec{e}_y + \frac{z - z_{i1} - (j-0.5)\Delta z_i}{r_{ij}}\vec{e}_z;$$

$$\vec{e}_r\,' = \frac{x - x_{i1} - (j-0.5)\Delta x_i}{r_{ij}'}\vec{e}_x + \frac{y + y_{i1} + (j-0.5)\Delta y_i}{r_{ij}'}\vec{e}_y + \frac{z - z_{i1} - (j-0.5)\Delta z_i}{r_{ij}'}\vec{e}_z,$$

where $\vec{e}_r$, $\vec{e}_r\,'$ – unit vectors corresponding to the direction from the middle of the line element and its mirror image to the observation point; $\vec{e}_x$, $\vec{e}_y$, $\vec{e}_z$ – unit vectors of the Cartesian coordinate system.

The magnetic field intensity of the system of short wires (Figure 5) is calculated using the Biot-Savart formula after calculating the power flow:

$$\dot{H}_i = \frac{\dot{I}_i}{4\pi r_i}(\cos\alpha_1 + \cos\alpha_2) \tag{10}$$

where $r_i = \sqrt{(x-x_a)^2 + (y-y_a)^2 + (z-z_a)^2}$; $r_{i1} = \sqrt{(x-x_1)^2 + (y-y_1)^2 + (z-z_1)^2}$;
$r_{i2} = \sqrt{(x-x_2)^2 + (y-y_2)^2 + (z-z_2)^2}$; $a = \sqrt{(x_a-x_1)^2 + (y_a-y_1)^2 + (z_a-z_1)^2}$

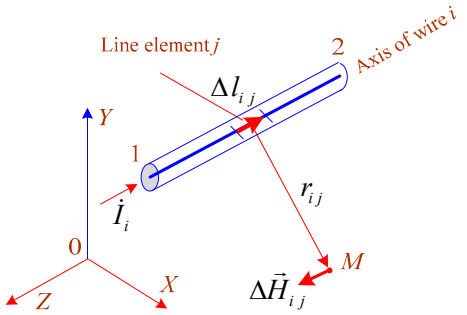

Figure 5. Magnetic field of a line element of the wire.

The positive current direction in Formula (10) corresponds to the direction from the start node 1 to the end node 2. The vector product has the following projections on the coordinate axes:

Preprints (www.preprints.org) | NOT PEER-REVIEWED | Posted: 6 June 2023 doi:10.20944/preprints202306.0400.v1

$$\Delta\vec{l}_{ij}=\frac{1}{n_i}\left[(x_{i2}-x_{i1})\,\vec{e}_x+(y_{i2}-y_{i1})\,\vec{e}_y+(z_{i2}-z_{i1})\,\vec{e}_z\right];$$

$$r_{ij}=\sqrt{[x_i+(j-0{,}5)\Delta x_i]^2+[y_i+(j-0{,}5)\Delta y_i]^2+[z_i+(j-0{,}5)\Delta z_i]^2}\;;$$

$$\vec{r}_{ij}=\frac{1}{r_{ij}}(x_{ij}\,\vec{e}_x+y_{ij}\,\vec{e}_y+z_{ij}\,\vec{e}_z);\;\; x_i=x_{i1}-x;\;\; y_i=y_{i1}-y;\;\; z_i=z_{i1}-z;$$

$$x_{ij}=x_i+(j-0{,}5)\Delta x_i;\;\; y_{ij}=y_i+(j-0{,}5)\Delta y_i;\;\; z_{ij}=z_i+(j-0{,}5)\Delta z_i;$$

$$\Delta x_i=(x_{i2}-x_{i1})/n_i;\;\; \Delta y_i=(y_{i2}-y_{i1})/n_i;\;\; \Delta z_i=(z_{i2}-z_{i1})/n_i;$$

$$\Delta\dot{H}_{ijX}=\frac{\dot{I}_i}{4\pi n_i r_{ij}^{\,3}}\left[(y_{i2}-y_{i1})\frac{z_{ij}}{r_{ij}}-(z_{i2}-z_{i1})\frac{y_{ij}}{r_{ij}}\right]; \tag{11}$$

$$\Delta\dot{H}_{ijY}=\frac{\dot{I}_i}{4\pi n_i r_{ij}^{\,3}}\left[(z_{i2}-z_{i1})\frac{x_{ij}}{r_{ij}}-(x_{i2}-x_{i1})\frac{z_{ij}}{r_{ij}}\right]; \tag{12}$$

$$\Delta\dot{H}_{ijZ}=\frac{\dot{I}_i}{4\pi n_i r_{ij}^{\,3}}\left[(x_{i2}-x_{i1})\frac{y_{ij}}{r_{ij}}-(y_{i2}-y_{i1})\frac{x_{ij}}{r_{ij}}\right]; \tag{13}$$

$$\dot{H}_X=\sum_{i=1}^{N1}\sum_{j=1}^{n_i}\Delta\dot{H}_{ijX};\;\; \dot{H}_Y=\sum_{i=1}^{N1}\sum_{j=1}^{n_i}\Delta\dot{H}_{ijY};\;\; \dot{H}_Z=\sum_{i=1}^{N1}\sum_{j=1}^{n_i}\Delta\dot{H}_{ijZ}\,. \tag{14}$$

Direction of vector $\Delta\vec{l}_{ij}$ is determined by the location of the points of beginning 1 and end 2 of the line element.

It is easier, however, to calculate the magnetic field of a short wire as a whole using the following formula (Figure 6):

$$\dot{H}_i=\frac{\dot{I}_i}{4\pi r_i}(\cos\alpha_1+\cos\alpha_2),$$

where $r_i=\sqrt{(x-x_a)^2+(y-y_a)^2+(z-z_a)^2}$; $r_{i1}=\sqrt{(x-x_1)^2+(y-y_1)^2+(z-z_1)^2}$;

$r_{i2}=\sqrt{(x-x_2)^2+(y-y_2)^2+(z-z_2)^2}$; $a=\sqrt{(x_a-x_1)^2+(y_a-y_1)^2+(z_a-z_1)^2}$.

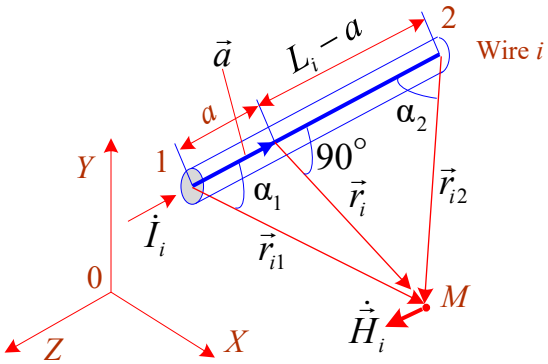

Figure 6. Magnetic field of the short wire.

To correctly determine the signs, the cosines of the angles α_1 and α_2 are calculated through scalar products of vectors

$$\cos\alpha_1=\frac{\vec{r}_{12}\cdot\vec{r}_{i1}}{r_{12}\cdot r_{i1}};\;\; \cos\alpha_2=-\frac{\vec{r}_{12}\cdot\vec{r}_{i2}}{r_{12}\cdot r_{i2}};$$

$$\vec{r}_{12}\cdot\vec{r}_{i1}=(x_2-x_1)(x-x_1)+(y_2-y_1)(y-y_1)+(z_2-z_1)(z-z_1);$$

$$\vec{r}_{12}\cdot\vec{r}_{i2}=(x_2-x_1)(x-x_2)+(y_2-y_1)(y-y_2)+(z_2-z_1)(z-z_2).$$

Coordinates of the beginning (x_a, y_a, z_a) of perpendicular r_i are determined by the equations of a straight line passing through the beginning and end of the wire, and a plane perpendicular to this line passing through the observation point M with coordinates (*x*, *y*, *z*)

Preprints (www.preprints.org) | NOT PEER-REVIEWED | Posted: 6 June 2023 doi:10.20944/preprints202306.0400.v1

$$\begin{cases} y_{21}(x_a - x_1) = x_{21}(y_a - y_1); \\ z_{21}(y_a - y_1) = y_{21}(z_a - z_1); \\ x_{21}(x_a - x) + y_{21}(y_a - y) + z_{21}(z_a - z) = 0, \end{cases}$$

where $x_{21} = x_2 - x_1$; $y_{21} = y_2 - y_1$; $z_{21} = z_2 - z_1$.

The coordinates of the point where the wire is divided by the perpendicular from the observation point at $x_{21} \neq 0$ are equal to

$$y_a = y_1 + \frac{y_{21}}{x_{21}}(x_a - x_1); \quad z_a = z_1 + \frac{z_{21}}{y_{21}}(y_a - y_1) = z_1 + \frac{z_{21}}{x_{21}}(x_a - x_1);$$

$$x_a = \frac{x_{21}x - y_{21}(y_1 - y) - z_{21}(z_1 - z) + x_1(y_{21}^2 + z_{21}^2)/x_{21}}{x_{21} + (y_{21}^2 + z_{21}^2)/x_{21}}.$$

There can be the following options:

1. $x_{21} = 0$; $y_{21} \neq 0$; $z_{21} \neq 0$.

$$x_a = x_1; \quad y_a = \frac{y_{21}z_{21}(z - z_1) + y_{21}^2 y + z_{21}^2 y_1}{y_{21}^2 + z_{21}^2}; \quad z_a = z - \frac{y_{21}}{z_{21}}(y_a - y).$$

2. $x_{21} = 0$; $y_{21} \neq 0$; $z_{21} = 0$; $x_a = x_1$; $y_a = y$; $z_a = z_1$.
3. $x_{21} = 0$; $y_{21} = 0$; $z_{21} \neq 0$; $x_a = x_1$; $y_a = y_1$; $z_a = z$.

Direction of vector $\dot{\vec{H}}_i$ is determined by the vector product $\vec{r}_{12} \times \vec{r}_{i1}$, where $\vec{r}_{12} = (x_2 - x_1)\,\vec{i} + (y_2 - y_1)\,\vec{j} + (z_2 - z_1)\,\vec{k}$ – vector of wire axis.

$$c_x = \frac{(\vec{r}_{12} \times \vec{r}_{i1})_x}{|\vec{r}_{12} \times \vec{r}_{i1}|} = \frac{c_{mx}}{c_m}; \quad c_y = \frac{(\vec{r}_{12} \times \vec{r}_{i1})_y}{|\vec{r}_{12} \times \vec{r}_{i1}|} = \frac{c_{my}}{c_m}; \quad c_z = \frac{(\vec{r}_{12} \times \vec{r}_{i1})_z}{|\vec{r}_{12} \times \vec{r}_{i1}|} = \frac{c_{mz}}{c_m};$$

$$c_m = \sqrt{c_{mx}^2 + c_{my}^2 + c_{mz}^2}; c_{mx} = (y_2 - y_1)(z - z_1) - (z_2 - z_1)(y - y_1);$$

$$c_{my} = (z_2 - z_1)(x - x_1) - (x_2 - x_1)(z - z_1); c_{mz} = (x_2 - x_1)(y - y_1) - (y_2 - y_1)(x - x_1);$$

$$\dot{H}_{ix} = \dot{H}_i c_x; \quad \dot{H}_{iy} = \dot{H}_i c_y; \quad \dot{H}_{iz} = \dot{H}_i c_z; \tag{15}$$

$$\dot{H}_x = \sum_{i=1}^{N1} \dot{H}_{ix}; \quad \dot{H}_y = \sum_{i=1}^{N1} \dot{H}_{iy}; \quad \dot{H}_z = \sum_{i=1}^{N1} \dot{H}_{iz}. \tag{16}$$

After the total values of the field intensity complexes are calculated using Formulas (9) and (16), one can determine the projections on the coordinate axes [28]. In particular, for the electric field

$$\vec{E}(t) = E_{mx}\sin(\omega t + \psi_x)\vec{e}_x + E_{my}\sin(\omega t + \psi_x)\,\vec{e}_y + E_{mz}\sin(\omega t + \psi_x)\,\vec{e}_z,$$

or

$$E_i(t) = E_{mi}\sin(\omega t + \psi_i), \quad i = x,\ y,\ z.$$

The square of the instantaneous value is

$$E^2(t) = \sum_{i=1}^{3}[E_{mi}\sin(\omega t + \psi_i)]^2 = \frac{1}{2}\sum_{i=1}^{3} E_{mi}^2[1 - \cos(2\omega t + 2\psi_i)];$$

$$E^2(t) = \frac{1}{2}\sum_{i=1}^{3} E_{mi}^2 + \frac{1}{2}\sin 2\omega t \sum_{i=1}^{3} E_{mi}^2 \sin 2\psi_i - \frac{1}{2}\cos 2\omega t \sum_{i=1}^{3} E_{mi}^2 \cos 2\psi_i.$$

Extreme points $E^2(t)$ are determined by the zeros of the derivative

$$\frac{\partial E^2(t)}{\partial t} = \frac{1}{2}\cos 2\omega t \sum_{i=1}^{3} E_{mi}^2 \sin 2\psi_i + \frac{1}{2}\sin 2\omega t \sum_{i=1}^{3} E_{mi}^2 \cos 2\psi_i = 0.$$

4. Modeling Results

The Fazonord software was used for modeling. EMF was calculated for two cases:

1) Short circuit of the contact wire to the rail;

Preprints (www.preprints.org) | NOT PEER-REVIEWED | Posted: 6 June 2023 doi:10.20944/preprints202306.0400.v1

2) Short circuit through the self-grounding resistance of the support.

Figures 7 and 8 show the model diagrams of modeling three-dimensional EMFs for the first and the second case respectively. The diagrams included models of the following components: 220 kV power transmission line; two traction substations with 40 MVA transformers; and a traction network of the intersubstation zone with a length of 50 km. In addition, models of the support of a catenary system and a system of short wires corresponding to the contact wire and rails were presented for modeling EMF according to the method presented in [28]. The conductivity of the earth was taken to be 0.01 S/m. The support was represented by four rods 10 m high, having the following x and z coordinates respectively: –5.5 m, –0.15 m; -5.2 m, –0.15 m; -5.5 m, 0.15 m; -5.2 m; 0.15 m. Self-grounding resistance R_S of a metal support is taken equal to 20 Ohm.

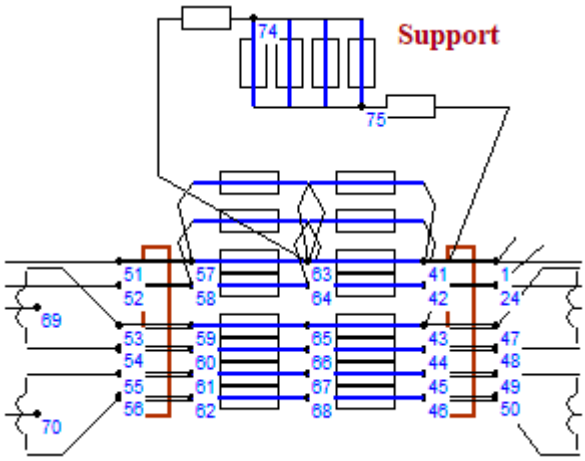

Figure 7. Model diagram for the case of contact wire short circuit to the rail.

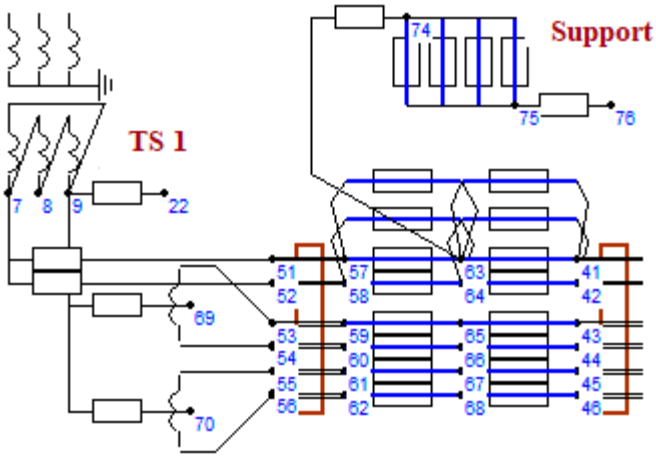

Figure 8. Model diagram for the case of a short circuit through the self-grounding resistance of the support.

The modeling yielded the *x*- and *z*- coordinate dependences of the intensity amplitudes for the electric and magnetic fields at a height of 1.8 m for contact wire short circuit to the rail (Figures 9–12), and for short circuit through the self-grounding resistance of the support (Figures 13–16). The spatial structure of the distribution of these parameters is shown in Figure 17—for the case of contact wire short circuit to the rail, and in Figure 18—for the short circuit through the self-grounding resistance of the support.

Preprints (www.preprints.org) | NOT PEER-REVIEWED | Posted: 6 June 2023 doi:10.20944/preprints202306.0400.v1

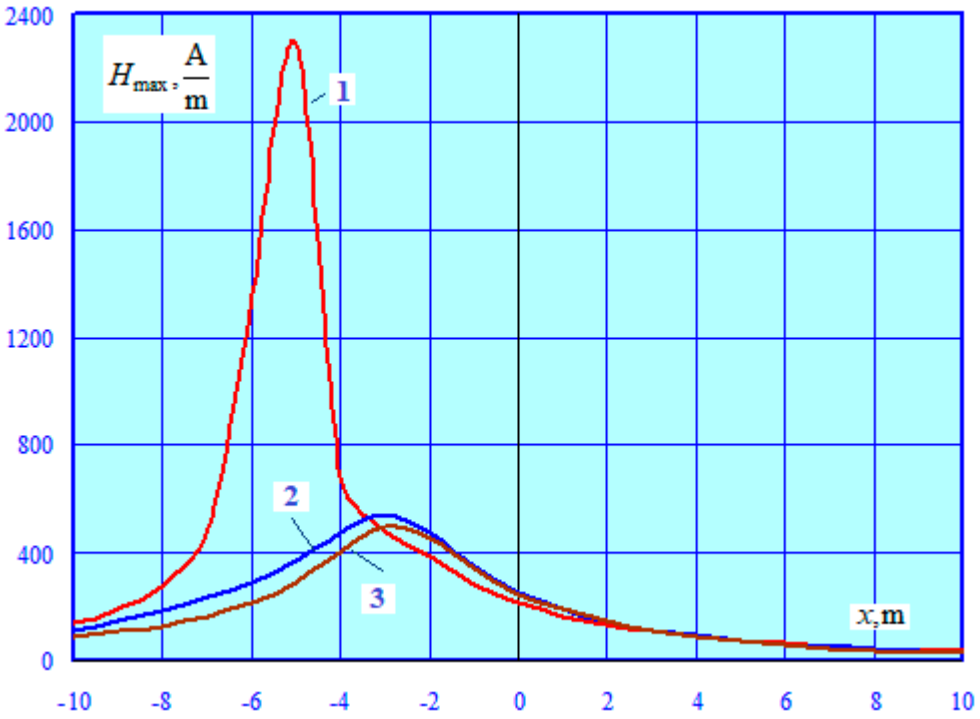

Figure 9. Magnetic field intensity amplitude $H_{max}(x)$ at a height of 1.8 m in the case of contact wire short circuit to the rail. A variation range of x: –10…10 m at: 1 – z = 0 m, 2 – z = 4 m, 3 – z = 8 m.

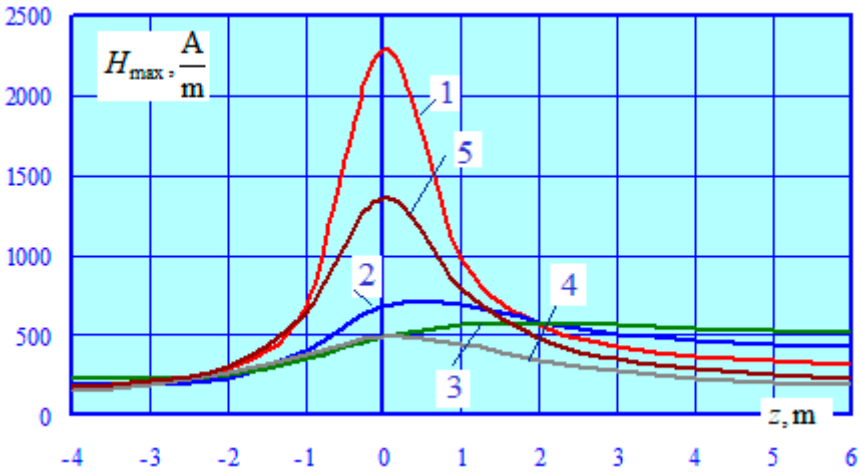

Figure 10. Magnetic field intensity amplitude $H_{max}(z)$ at a height of 1.8 m in the case of contact wire short circuit to the rail. A variation range of z: -4 ... 6 m at: 1 - x = -5 m, 2 - x = - 4 m, 3 - x = - 3 m, 4 - x = - 7 m, 5 – x = - 6 m.

Preprints (www.preprints.org) | NOT PEER-REVIEWED | Posted: 6 June 2023 doi:10.20944/preprints202306.0400.v1

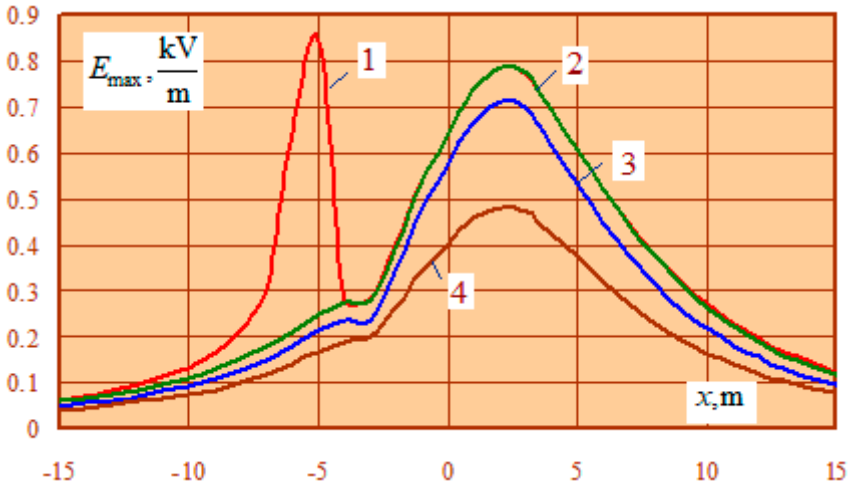

Figure 11. Electric field intensity amplitude $E_{max}(x)$ at a height of 1.8 m in the case of contact wire short circuit to the rail. A variation range of x: -15 ... 15 m at: 1 - z = 0 m, 2 - z = 8 m, 3 - z = 16 m, 4 - z = 20 m.

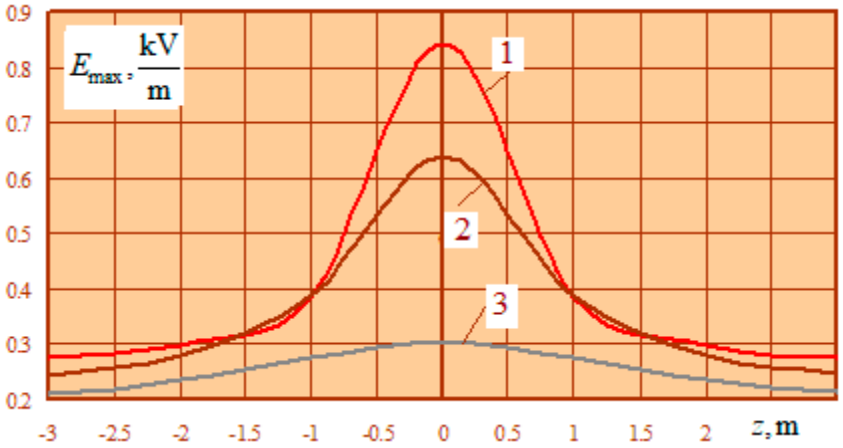

Figure 12. Electric field intensity amplitude $E_{max}(z)$ at a height of 1.8 m in the case of contact wire short circuit to the rail. A variation range of z: –3…3 m at: 1 –x = – 5 m, 2 – x = – 7 m, 3 – x = – 6 m.

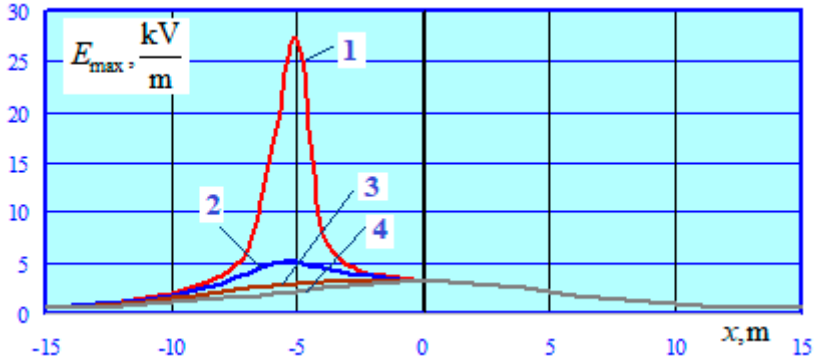

Figure 13. Electric field intensity amplitude $E_{max}(x)$ at a height of 1.8 m for a short circuit through the self-grounding resistance of the support. A variation range of x: –15…15 m; 1 – z = 0 m, 2 – z = 2 m, 3 – z = 4 m, 4 – z = 8 m.

Preprints (www.preprints.org) | NOT PEER-REVIEWED | Posted: 6 June 2023 doi:10.20944/preprints202306.0400.v1

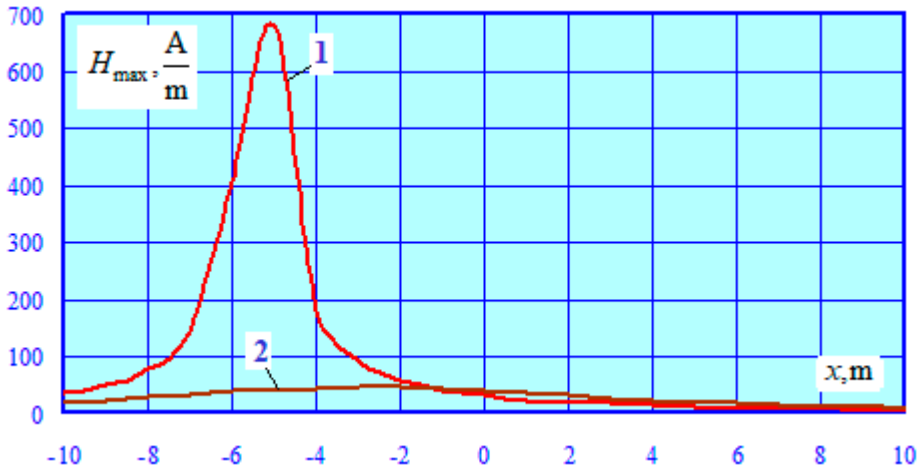

Figure 14. Magnetic field intensity amplitude $H_{max}(x)$ at a height of 1.8 m for a short circuit through the self-grounding resistance of the support. A variation range of x: –10…10 m; 1 – z = 0 m, 2 – z = 4 m.

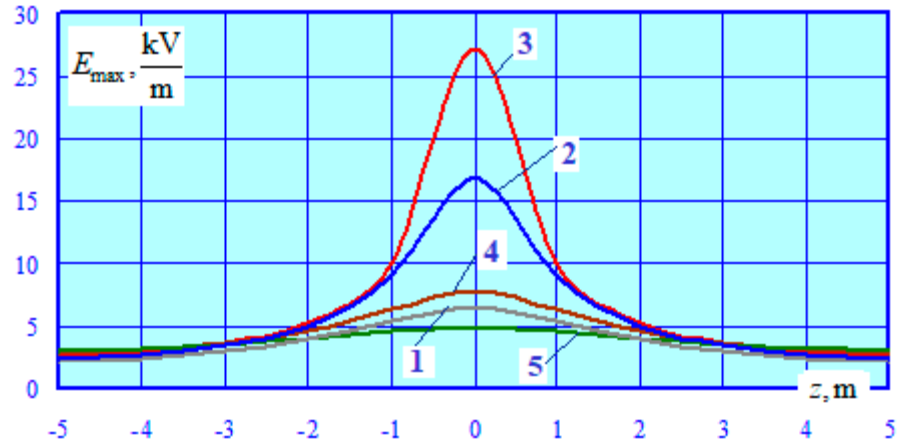

Figure 15. Electric field intensity amplitude $E_{max}(z)$ at a height of 1.8 m for a short circuit through the self-grounding resistance of the support. A variation range of z: –5…5 m; 1 – x = –7 m, 2 – x = –6 m, 3 – x = –5 m, 4 – x = –4 m, 5 – x = –3 m.

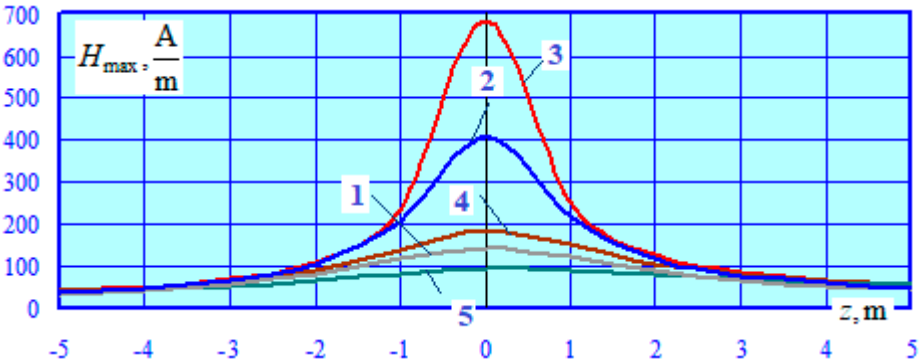

Figure 16. Magnetic field intensity amplitude $H_{max}(z)$ at a height of 1.8 m for a short circuit through the self-grounding resistance of the support. A variation range of x –5 … 5 m; 1 – x = –7 m, 2 – x = –6 m, 3 – x = –5 m, 4 – x = –4 m, 5 – x = –3 m.

Preprints (www.preprints.org) | NOT PEER-REVIEWED | Posted: 6 June 2023 doi:10.20944/preprints202306.0400.v1

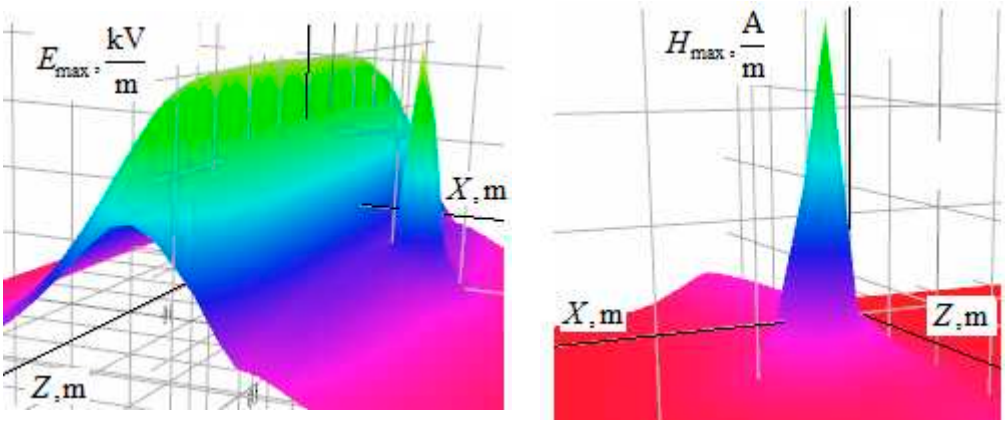

a) b)

Figure 17. Spatial structure of intensity distribution for the electric (a) and magnetic (b) fields in the case of the contact wire short circuit to the rail.

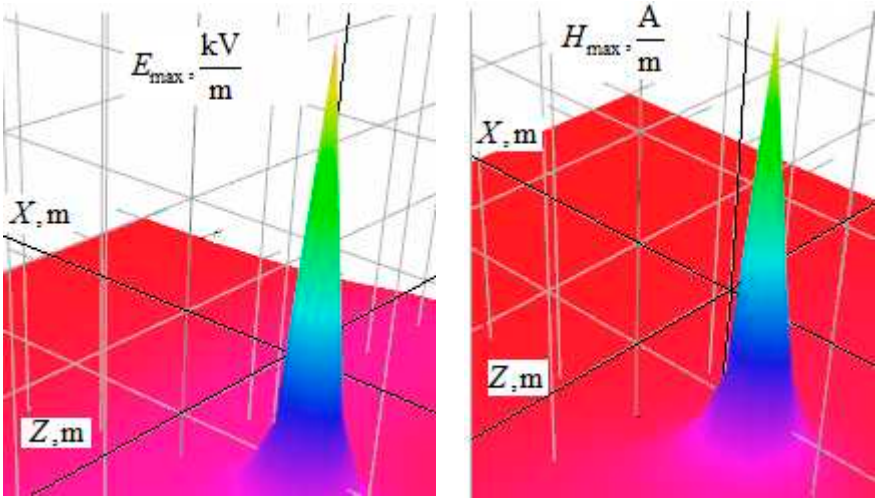

Figure 18. The spatial structure of the intensity distribution for the electric (a) and magnetic (b) fields in the case of a short circuit through the self-grounding resistance of the support.

5. Discussion of Modeling Results

The data capturing the modeling results are shown in Figures 19–22.

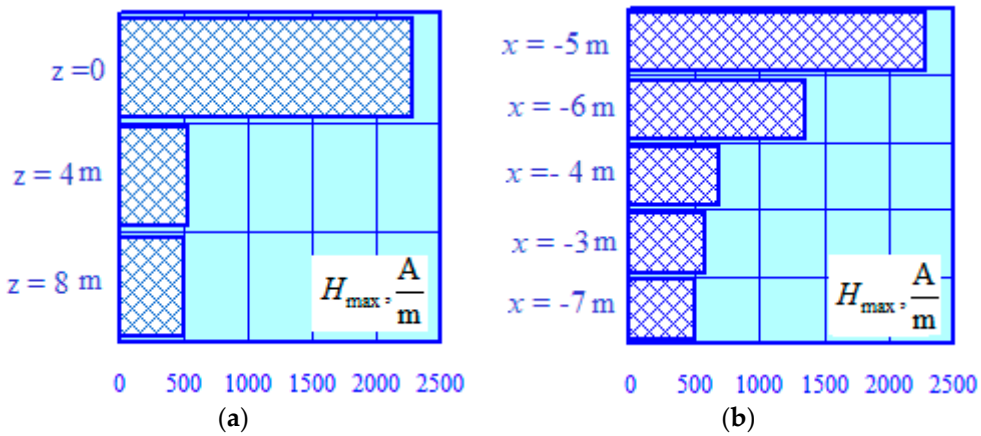

Preprints (www.preprints.org) | NOT PEER-REVIEWED | Posted: 6 June 2023 doi:10.20944/preprints202306.0400.v1

Figure 19. Maximum amplitudes of the magnetic field intensity $H_{max}(x)$ for the short circuit of contact wire to the rail. A variation range of x: = –10…10 m (a), a variation range of z = –4 … 6 m (b).

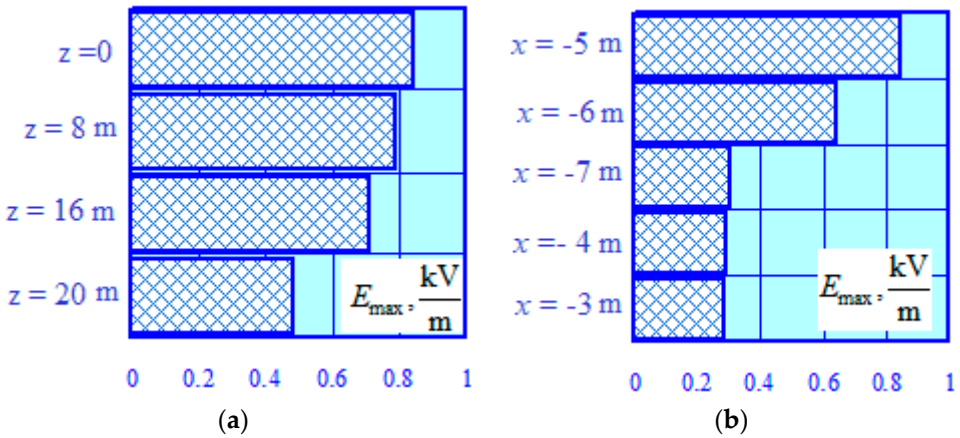

Figure 20. Maximum amplitudes of the electric field intensity $E_{max}(x)$ for the short circuit of contact wire to the rail. A variation range of x: –15…15 m (a), a variation range of z: –3…3 m (b).

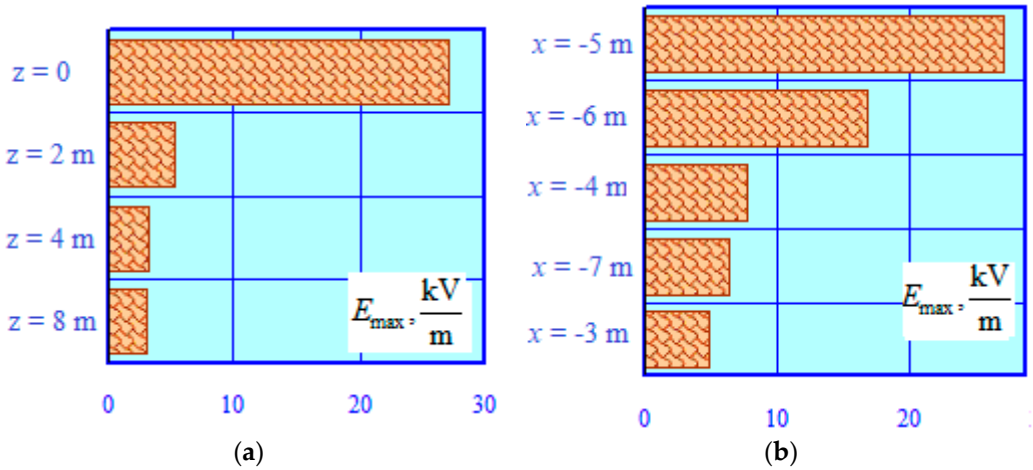

Figure 21. Maximum amplitudes of the electric field intensity E_{max} for a short circuit through the self-grounding resistance of the support. A variation range of x: –15…15 m (a), a variation range of z: –5…5 m (b).

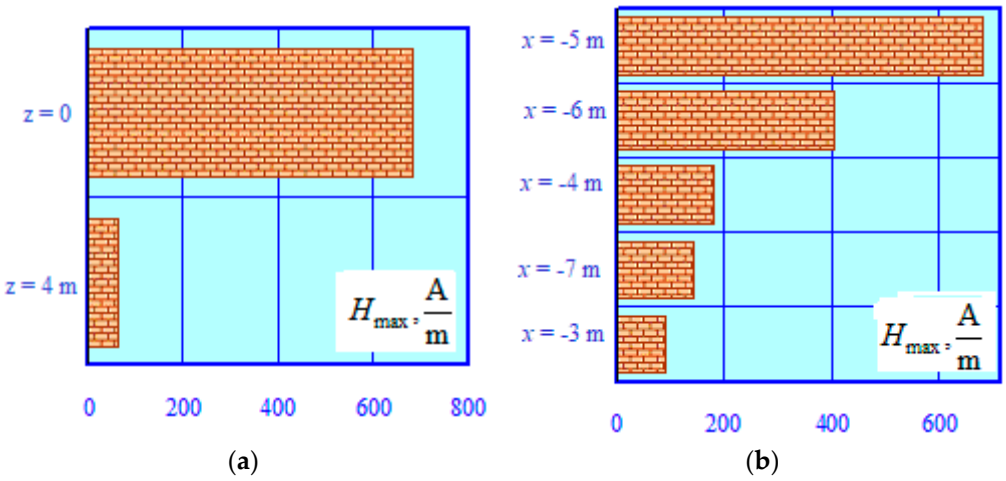

Figure 22. Maximum amplitudes of the magnetic field intensity H_{max} for a short circuit through the self-grounding resistance of the support. A variation range of x: –10…10 m (a), a variation range of z: –5…5 m (b).

The findings of the research indicate that:

– The maximum value of the amplitude of the magnetic field intensity in the case of contact wire short circuit to the rail reaches 2.3 kA/m near the support, which can cause malfunction of electronic equipment; the same parameter for the electric field is 0.84 kV/m and does not exceed the allowable values;
– The three-dimensional electromagnetic field in the case of a contact wire short circuit through the support to the rail and a short circuit through the self-grounding resistance of the support has a complex spatial structure;
– There is a significant increase in EMF intensity near the support; for example, the magnetic field intensity in the case of a short circuit through the self-grounding resistance of the support reaches 683 A/m, and the electric field intensity for the same short circuit is 27 kV/m;
– As the distance from the support increases, the intensity levels go down fast.

6. Conclusions

The paper presents an approach developed to correctly factor in the influence of supports in modeling electromagnetic fields of traction networks of mainline railways. Its main feature is that all single-wire objects of the model diagram (support rods and a system of short wires corresponding to contact wires of catenary system and rails) constitute a single group of components that create a field; the EMF is determined on the basis of the power flow calculation in phase coordinates.

The approach is implemented in the commercial software Fazonord, is universal and can be used to determine electromagnetic fields at any electric power facilities, which include current-carrying parts of a limited length. It can be used:

- to determine electromagnetic fields near supports of overhead power lines and traction networks of various designs;
- to calculate EMF intensities at substations;
- to factor in the influence of metal objects located near the traction network, for example, pedestrian crossings at railway stations.

Funding: The research was carried out within the framework of the state task “Conducting applied scientific research” on the topic “Development of methods, algorithms and software for modeling the modes of traction power supply systems for DC railways and electromagnetic fields at traction substations for AC railways”.

References

1. B. Blake Levit. Electromagnetic Fields: A Consumer’s Guide to the Issues and How to Protect Ourselves. iUniverse. 462 p.
2. Natalya V. Buyakova, Vasiliy P. Zakaryukin, Dmitriy A. Seredkin. Simulation of Electromagnetic Fields Generatedby Overhead Power Lines and Railroad Traction Networks. Energy Systems Research, Vol. 4, No. 2, 2021. pp. 70-88.
3. B. Ali Rachedi, A. Babouri, F. Berrouk. A study of electromagnetic field generated by high voltage lines using COMSOL MULTIPHYSICS. 2014 International Conference on Electrical Sciences and Technologies in Maghreb (CISTEM). Publisher: IEEE.
4. J. Liu; W. Ruan; S. Fortin; F.P. Dawalibi. Electromagnetic fields near high voltage electrical power lines: a parametric analysis. 2002 Proceedings. International Conference on Power System Technology. Publisher: IEEE.
5. S.M. Al Dhalaan; M.A. Elhirbawy. A quantitative study of the electromagnetic field coupling between electric power transmission line and railway. CCECE 2003 - Canadian Conference on Electrical and Computer Engineering. Toward a Caring and Humane Technology. Publisher: IEEE.
6. O. Sougui and M. Z. b. Mohd Jenu, “Measurement and analysis of magnetic field radiation near 132KV power lines,” 2014 IEEE Asia-Pacific Conference on Applied Electromagnetics (APACE), 2014, pp. 207-210, doi: 10.1109/APACE.2014.7043781. Publisher: IEEE.
7. S. Mahapatra, T. K. Dey and J. Ghosh, “Estimation of the fields radiated from H.T. power lines,” 2008 10th International Conference on Electromagnetic Interference & Compatibility, 2008, pp. 395-397. Publisher: IEEE.
8. L. Xiao and K. E. Holbert, “Development of software for calculating electromagnetic fields near power lines,” 2014 North American Power Symposium (NAPS), 2014, pp. 1-6, doi: 10.1109/NAPS.2014.6965378. Publisher: IEEE.

9. M. Purcar, C. Munteanu, A. Avram and F. Miron, "CAD/CAE modeling of electromagnetic field distribution in hv substations and investigation of the human exposure," 2016 International Conference on Applied and Theoretical Electricity (ICATE) , 2016, pp. 1-5, doi: 10.1109/ICATE.2016.7754698. Publisher: IEEE.
10. L. Xu, Y. Li, J. Yu, X. Hou and C. An, "Research on Electric Field of High-Voltage Transmission Line Power Frequency," 2006 International Conference on Power System Technology , 2006, pp. 1-4, doi: 10.1109/ICPST.2006.321493. Publisher: IEEE.
11. H. Das, K. Gogoi and S. Chatterjee, "Analysis of the effect of electric field due to High Volt-age Transmission lines on humans," 2015 1st Conference on Power, Dielectric and Energy Management at NERIST (ICPDEN), 2015, pp. 1-4, doi: 10.1109/ICPDEN.2015.7084491. Publisher: IEEE.
12. F. Wang, W. Wang, Z. Jiang and X. Zhao, "Analysis of the Line-Frequency Electric Field Intensity around EHV Transmission," 2010 International Conference on Electrical and Control Engineering, 2010, pp. 3343-3346, doi: 10.1109/iCECE.2010.815. Publisher: IEEE.
13. B. Yang, S. Wang, Q. Wang, H. Du and Y. Huangfu, "Simulation and analysis for power frequency electric field of building close to power transmission lines," 2014 IEEE International Symposium on Electromagnetic Compatibility (EMC), 2014, pp. 451-454, doi: 10.1109/ISEMC.2014.6899014. Publisher: IEEE.
14. C. D. Oancea, F. Calin and V. Golea, "On the Electromagnetic Field in the Surrounding Area of Railway Equipment and Installations," 2019 International Conference on Electromechanical and Energy Systems (SIELMEN), Craiova, Romania, 2019, pp. 1-5, doi: 10.1109/SIELMEN.2019.8905871.
15. B. Bat-Erdene, M. Battulga and G. Tuvshinzaya, "Method Of Calculation Of Low-Frequency Electromagnetic Field Around 15 kV Transmission Lines," 2020 IEEE International Conference on Power and Energy (PECon), Penang, Malaysia, 2020, pp. 40-43, doi: 10.1109/PECon48942.2020.9314436.
16. I. Duane, M. Afonso, A. Paganotti and M. A. O. Schroeder, "Computation of the Electromagnetic Fields of Overhead Power Lines with Boundary Elements," 2022 IEEE 20th Biennial Conference on Electromagnetic Field Computation (CEFC), Denver, CO, USA, 2022, pp. 1-2, doi: 10.1109/CEFC55061.2022.9940848.
17. D. Medveď, J. Zbojovský, M. Pavlík, I. Kolcunová and J. Urbanský, "Comparison of Electromagnetic Fields around Electric Power Lines," 2020 21st International Scientific Conference on Electric Power Engineering (EPE), Prague, Czech Republic, 2020, pp. 1-6, doi: 10.1109/EPE51172.2020.9269217.
18. X. Zeng et al., "Research on electromagnetic radiation of Xijiang traction substation," 2018 IEEE International Symposium on Electromagnetic Compatibility and 2018 IEEE Asia-Pacific Symposium on Electromagnetic Compatibility (EMC/APEMC), Suntec City, Singapore, 2018, pp. 24-27, doi: 10.1109/ISEMC.2018.8393731.
19. C. D. Oancea, F. Calin and V. Golea, "Analysis of the Influences of the Electromagnetic Field Produced by an Electrified Railway Section," 2020 7th International Conference on Energy Efficiency and Agricultural Engineering (EE&AE), Ruse, Bulgaria, 2020, pp. 1-6, doi: 10.1109/EEAE49144.2020.9279005.
20. S. M. Ghania, "Fuzzy prediction of the electromagnetic fields inside high voltage substations," 2016 IEEE International Conference on High Voltage Engineering and Application (ICHVE), Chengdu, China, 2016, pp. 1-4, doi: 10.1109/ICHVE.2016.7800809.
21. J. A. Morales, P. Gavela and A. S. Bretas, "Electromagnetic fields in distribution feeders and electrical substations analysis: A study case in Ecuador," 2015 North American Power Symposium (NAPS), Charlotte, NC, USA, 2015, pp. 1-6, doi: 10.1109/NAPS.2015.7335084.
22. S. Nikolovski, Z. Klaić, Z. Kraus and M. Stojkov, "Computation and measurement of electromagnetic fields in high voltage transformer substations," The 33rd International Convention MIPRO, Opatija, Croatia, 2010, pp. 641-646.
23. Ogunsola A. and Mariscotti A. Electromagnetic Compatibility in Railways. Springer-Verlag Berlin Heidelberg 2013, 568 pp.
24. Luan Xiaotian, Zhu Haijing, Qiu Bo, Han Bochong. EMC in Rail Transportation. CUE2016-Applied Energy Symposium and Forum 2016: Low carbon cities & urban energy systems. Available online at www.sciencedirect.com.
25. Kircher R., Klühspies J., Palka R., et al. Electromagnetic Fields Related to High Speed Transportation Systems. Transportation Systems and Technology. 2018; 4(2):152-166.
26. Baranowski S., Ouaddi H., Kone L. and Idir N. EMC Analysis of Railway Power Substation Modeling and Measurements Aspects. Infrastructure Design, Signalling and Security in Railway. InTech, Available from www.intechopen.com.
27. Lu Zhang, Yun Zhu, Song Chen, Dan Zhang. Simulation and Analysis for Electromagnetic Environment of Traction Network. 2021 XXXIVth General Assembly and Scientific Symposium of the International Union of Radio Science (URSI GASS). 2021 Publisher: IEEE.
28. Zakaryukin V.P., Kryukov A.V. Modeling of Electromagnetic Fields Generated by a System of Short Current-carrying Parts / System Analysis and Mathematical Modeling. No. 2. 2021. pp. 145-163.

 doi:10.20944/preprints202306.0400.v1

29. V. P. Zakaryukin and A. V. Kryukov, Complex Asymmetric Conditions of Electrical Systems. Irkutsk, 2005. 273 p.
30. Kosarev A.B., Kosarev B.I. Fundamentals of Electromagnetic Safety of Railway Transport Power Supply Systems. Moscow: Intext, 2008. 480 p.
31. Carson J.R. Wave propagation in overhead wires with ground return. Bell Syst. Tech. J., 1926, 5, pp. 539–554.
32. Kostenko M.V. Wave processes and electrical noise in multi-wire high voltage lines / M.V. Kostenko, L.S. Perelman, Yu.P. Shkarin. Moscow: Energia Publ., 1973. 272 p.